Electron excitation after plasmon decay in proton-aluminum collisions

G. Bocan and J. E. Miraglia

Instituto de Astronomía y Física del Espacio, Consejo Nacional de Investigaciones Científicas y Técnicas, Agencia Nacional para la Promoción de la Ciencia y la Tecnología, Departamento de Física, Facultad de Ciencias Exactas y Naturales, Universidad de Buenos Aires, C.C. 67, Sucursal 28, 1428 Buenos Aires, Argentina

(Received 12 November 2002; published 21 March 2003)

When a projectile travels inside a metal, it interacts with the electron gas, producing both binary and collective excitations (plasmons). Within the nearly-free-electron-gas scheme, Rösler and co-workers showed that plasmons decay in first order and a conduction electron is emitted (interband transition). Working within the frame of atomic collisions, we develop a simple model to describe this decay. The first-order Born expansion is used to approximate the electron wave functions. The influence of the lattice potential on the excited electron is considered in the calculations in order to balance the momentum-conservation equation. It gives contributions associated with sites of the reciprocal lattice. The potential expansion coefficients are obtained following Animalu and co-workers [Philos. Mag. **9**, 451 (1964)]. First- and second-differential spectra (in energy and angle) are analyzed discriminating contributions due to different lattice momenta. In all cases, contributions due to binary excitations of the valence electrons and inner-shell ionization are presented to establish a comparison.

DOI: 10.1103/PhysRevA.67.032902 PACS number(s): 79.20.Ap, 34.10.+x

I. INTRODUCTION

There are several mechanisms through which a projectile traveling inside a metal can interact with the metal electron gas. These interactions result both in binary and collective excitations [1]. The latter are usually referred to as ''plasmons.'' In real metals, these plasmons have a finite lifetime and eventually decay. Chung and Everhart showed in 1977 [2] that, within the nearly-free-electron-gas (NFEG) model, an important source of emitted low-energy secondary electrons may arise from the decay of long-wavelength surface and volume plasmons via near vertical interband transitions. Later on, Rösler and co-workers [3–6] continued their work considering not only secondary electron emission but also particle-induced one. In a series of publications, they developed most of the theory presently available on plasmon decay and its contribution to the electron emission spectra. Working with NFE metals and within a model potential formalism (developed by Animalu and co-workers [7–11]), they showed that the excitation of conduction electrons by decay of plasmons generated by the impinging particle results in an important contribution to the electron emission.

In this paper, a simple model is developed to describe plasmon decay via interband transitions. The electron gas is assumed to be under the influence of a weak periodic potential due to the lattice. This potential can be expanded in plane waves with definite momenta $\mathbf{G}$ that correspond to the sites of the reciprocal lattice (bcc for Al) [12]. The expansion coefficients are $V_{\mathbf{G}}$ and are tabulated [11]. The excited electron wave function is approximated using a first-order Born expansion. Calculations are kept to first order in Z_P (charge of the projectile) and in V (the lattice potential). We follow a simple derivation arriving an expression equivalent to the one obtained by Rösler and co-workers. These authors worked with the two lowest values of $\mathbf{G}$ (namely, $\mathbf{G}_1$ and $\mathbf{G}_2$), although some considerations regarding $\mathbf{G}_3$ can be found in a paper by Rösler and Brauer [13]. In our calculations, $\mathbf{G}_3$ contributions are included and turn out to be relevant.

In Sec. II, the model is derived and the approximations involved in the model are explained. In Sec. III, the results of our numerical calculations are shown and analyzed. Total probabilities as well as stopping powers are presented. Also, single- and double-differential spectra are obtained in terms of both the excited electron final energy and its final moving direction (with respect to the projectile's initial velocity). All calculations are performed for polycrystalline Al penetrated by protons. Atomic units are used throughout this paper.

II. THEORY

A. The transition matrix

The total Hamiltonian of a projectile moving in an NFEG can be written as $H=H_0+V$,

$$H_0=-\frac{1}{2M_P}\nabla_{\mathbf{R}}^2-\sum_j \frac{1}{2}\nabla_{\mathbf{r}_j}^2,$$

$$V=V^{(P)}+V^{(e)}+V^{(S)}=\sum_j (V_j^{(P)}+V_j^{(e)}+V_j^{(S)}), \qquad (1)$$

where $V_j^{(P)}=-Z_P/|\mathbf{R}-\mathbf{r}_j|$ is the projectile-electron Coulomb attraction, $V_j^{(e)}=\Sigma_l'(1/|\mathbf{r}_l-\mathbf{r}_j|)$ is the electron-electron repulsion, and $V_j^{(S)}=\Sigma_l W(\mathbf{X}_l-\mathbf{r}_j)$ is the attractive interaction of the electron with the whole solid crystal composed by the ions cores. Coordinates $\mathbf{R}$, $\mathbf{r}_j$, and $\mathbf{X}_l$ represent the projectile, electron, and ion-core positions, respectively.

In general, the initial and final Hartree states of the many-electron system are simply

$$\Psi_i=\Phi_{\mathbf{K}_i}\phi_{\mathbf{k}_{i1}}\phi_{\mathbf{k}_{i2}}\cdots\xi_{ij}^{+}\cdots, \qquad (2)$$

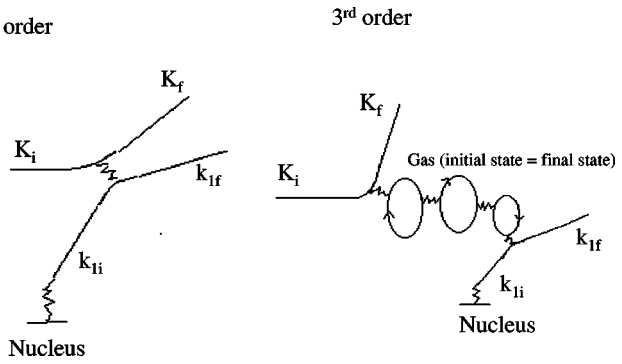

FIG. 1. Schematic diagram of the interactions. A first-order contribution is shown.

$$\Psi_f = \Phi_{\mathbf{K}_f} \phi_{\mathbf{k}_{f1}} \phi_{\mathbf{k}_{f2}} \cdots \xi^{-}_{fj} \cdots,$$

where we have singled out the excited electron (named "j") by the wave functions $\xi_{(i,f)j}$ satisfying

$$\left[-\frac{1}{2}\nabla^2_{\mathbf{r}_j} + V_j^{(S)} + V_j^{(e)} - \varepsilon_{(i,f)} \right] \xi^{(+,-)}_{(i,f)j} = 0. \tag{3}$$

The other electrons as well as the projectile will be considered as free particles. Their wave functions ($\phi_{\mathbf{k}}$ and $\Phi_{\mathbf{K}}$), are plane waves (normalized to the Dirac δ), thus neglecting $V_l^{(S)} + V_l^{(e)}$ for $l \neq j$. Further, we will focus on the case when the free-electron final states are such that $\phi_{\mathbf{k}_{f1}} = \phi_{\mathbf{k}_{i1}}, \phi_{\mathbf{k}_{f2}} = \phi_{\mathbf{k}_{i2}} \cdots$ (see Fig. 1), that is, the bulk ends in its ground state.

We build the Born series for the T-matrix element corresponding to the ejection of the electron j as: $T_j = \Sigma_m T_j^{(m)}$, where $T_j^{(1)} = \langle \Psi_f | V | \Psi_i \rangle = \langle \Psi_f | V_j^{(P)} | \Psi_i \rangle$ is the first Born approximation, $T_j^{(2)} = \langle \Psi_f | (V_j^{(P)} + V_j^{(e)}) G^{+}_{j0} (V_j^{(P)} + V_j^{(e)}) | \Psi_i \rangle$ is the second one, etc. The operator $G^{\pm}_{j0}$ is the usual free Green's operator containing the interaction of the solid with the ejected electron, i.e.,

$$G^{+}_{j0} = [E - H_0 - V_j^{(S)} + i0^{+}]^{-1}, \tag{4}$$

where

$$E = \frac{1}{2M_P} K_i^2 + \varepsilon_i = \frac{1}{2M_P} K_f^2 + \varepsilon_f \tag{5}$$

is the total energy, and M_P is the projectile heavy mass ($M_P \gg 1$). The T-matrix element in Born first-order approximation is very simple (see Fig. 1), and reads

$$T_j^{(1)} = \tilde{V}_P(\mathbf{q}) F_{fi}(\mathbf{q}), \tag{6}$$

where $\mathbf{q} = \mathbf{K}_i - \mathbf{K}_f$ is the projectile momentum transfer, $\tilde{V}_P(\mathbf{q}) = -Z_P 4\pi/q^2$, and $F_{fi}(\mathbf{q})$ is the electronic form factor,

$$F_{fi}(\mathbf{q}) = \langle \xi^{-}_{fj} | \exp(i\mathbf{q}\cdot\mathbf{r}) | \xi^{+}_{ij} \rangle. \tag{7}$$

Higher Born terms to first order in Z_P can be calculated in closed forms, and give

$$T_j^{(m)} = T_j^{(1)} [X(q, \mathbf{q}\cdot\mathbf{v})]^m + O(Z_P^2), \tag{8}$$

$$X(q,\omega) = \frac{4\pi}{q^2} \int \frac{d\mathbf{k}}{(2\pi)^{3/2}} \Theta(k_F - k)[g^{+} + g^{-}], \tag{9}$$

$$g^{\pm} = \left[\frac{1}{2}\mathbf{k}^2 - \frac{1}{2}(\mathbf{q} \pm \mathbf{k})^2 \pm (\omega + i\eta) \right]^{-1}. \tag{10}$$

The Born series can be then summed up to all orders in the electron-electron (e-e) repulsion to give the simplest Padé approximant

$$T_j = \sum_j T_j^{(m)} = \tau(\mathbf{q}) F_{fi}(\mathbf{q}), \tag{11}$$

$$\tau(\mathbf{q}) = \tilde{V}_P(\mathbf{q}) \frac{1}{\varepsilon_L(q,\omega)}, \tag{12}$$

where $\varepsilon_L(q,\omega) = 1 - X(q,\omega)$ is the well-known Lindhard dielectric response function [14,15]. Finally, we have to add on j, or $\Sigma_j \equiv 2\int d\mathbf{k}_i \Theta(k_F - k_i)$. To proceed further, we need the Fermi golden rule to compute the differential probability per unit time of electron excitation due to plasmon decay dP_t^{Dec} as

$$\frac{dP_t^{Dec}}{d\mathbf{q} d\mathbf{k}_i d\mathbf{k}_f} = 2\pi \delta(\mathbf{v}\cdot\mathbf{q} + \varepsilon_i - \varepsilon_f) |\tau(\mathbf{q}) F_{fi}(\mathbf{q})|^2, \tag{13}$$

and it is similar to the result obtained by Chung and Everhart [2].

B. The form factor

In binary projectile-electron collisions, the role of the solid is neglected, and the ejected electrons are described as free particles, $\xi^{(+,-)}_{(i,f)} = \phi_{\mathbf{k}_{(i,f)}}$. The form factor reduces to $\langle \phi_{\mathbf{k}_f} | \exp(i\mathbf{q}\cdot\mathbf{r}) | \phi_{\mathbf{k}_i} \rangle = \delta(\mathbf{q} - \mathbf{p})$, with $\mathbf{p} = \mathbf{k}_f - \mathbf{k}_i$, and, to first order [16], the T-matrix element is given simply by

$$T^{Bin} = \delta(\mathbf{q} - \mathbf{p}) \tau(\mathbf{q}). \tag{14}$$

To study the role of the lattice in plasmon decay, we consider a weak periodic potential $V^{(S)}$ acting on the electrons. This potential is due to the ion cores, and can be expanded as follows:

$$V^{(S)}(\mathbf{r}) = \sum_{\mathbf{G}} V_{\mathbf{G}} e^{i\mathbf{G}\cdot\mathbf{r}}, \tag{15}$$

where $\mathbf{G}$ is a vector pointing to a site in the reciprocal lattice.

Keeping our calculations to first order in the potential, the Bethe expansion [17] for the form factor [Eq. (7)] gives

$$F_{fi}(\mathbf{q}) = \delta(\mathbf{q} - \mathbf{p}) + V_{\mathbf{G}} \left(\frac{1}{D_{0i}} + \frac{1}{D_{0f}} \right), \tag{16}$$

with

$$D_{0i} = \omega_{\mathbf{k}_i} - \omega_{\mathbf{k}_f - \mathbf{q}} + i0^{+}, \tag{17}$$

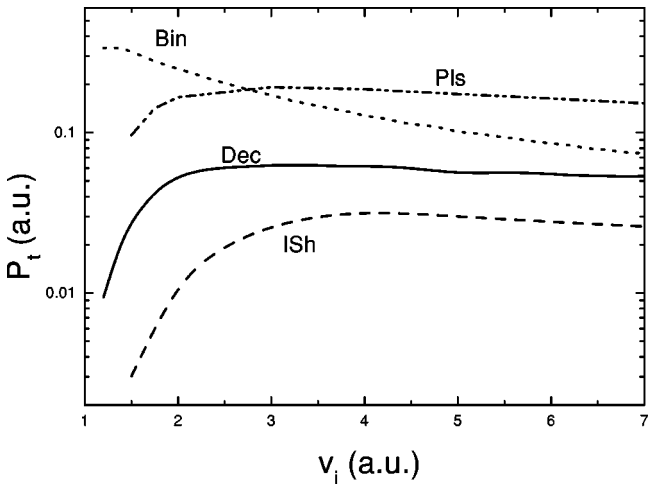

FIG. 2. Total probability per unit time as a function of the projectile initial velocity for the three processes ending with an electron in the continuum. Plasmon decay is plotted with a solid line, binary contribution with a dotted line, and inner-shell contribution with a dashed line. Plasmon excitation is added to the plot with the dash-double-dotted line.

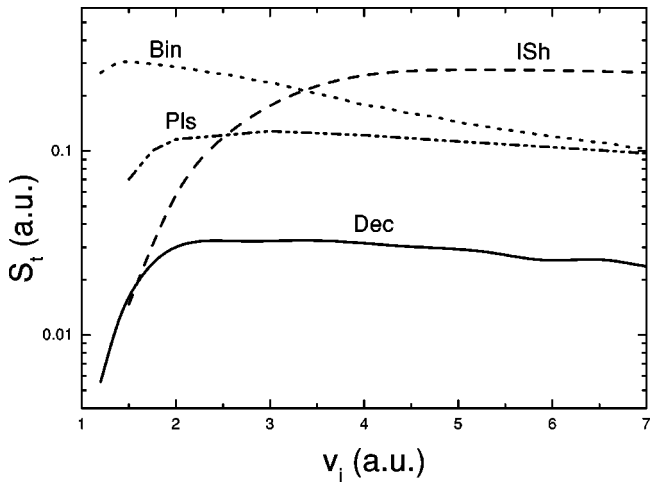

FIG. 3. Stopping power per unit time as a function of the projectile initial velocity for the three processes considered in Fig. 2 as well as for plasmon excitation. The notation is similar to Fig. 2.

$$D_{0f}=\omega_{\mathbf{k}_f}-\omega_{\mathbf{k}_i+\mathbf{q}}+i0^+, \tag{18}$$

where $\omega_{\mathbf{k}}=\mathbf{k}^2/2(\varepsilon_i=\omega_{\mathbf{k}_i},\varepsilon_f=\omega_{\mathbf{k}_f})$. The first term of Eq. (16) represents the momentum-conservation in a binary projectile-electron collision as mentioned above. The second term represents the situations in which the lattice takes part in the momentum-conservation equation. Thus the probability per unit time for given $\mathbf{k}_i$ and $\mathbf{k}_f$, and to the lowest order in $V_{\mathbf{G}}$ reduces to

$$\frac{dP_t^{Dec}}{d\mathbf{k}_i d\mathbf{k}_f}=2\pi\sum_{\mathbf{G}}\ \delta(\mathbf{v}\cdot\mathbf{q}+\varepsilon_i-\varepsilon_f)\,\delta(\mathbf{G}-\mathbf{p}+\mathbf{q}) \times|V_{\mathbf{G}}|^2|\tau(-\mathbf{G}+\mathbf{p})|^2\left|\frac{1}{D_{0i}}+\frac{1}{D_{0f}}\right|^2. \tag{19}$$

Note that the lattice absorbs momentum but not energy.

The second δ function implies $\mathbf{K}_i+\mathbf{k}_i=\mathbf{K}_f+\mathbf{k}_f+\mathbf{G}$ and accounts for the momentum conservation. The differential cross section of the excited electron per unit time is

$$\frac{dP_t^{Dec}}{d\mathbf{k}_f}=2\int d\mathbf{k}_i\left(\frac{dP_t^{Dec}}{d\mathbf{k}_i d\mathbf{k}_f}\right)\Theta(k_F-k_i), \tag{20}$$

and the total cross section is simply the integration of dP_t^{Dec} on $d\mathbf{k}_f$.

C. The degeneracy at the Bragg plane

If $|\mathbf{k}_i|=|\mathbf{k}_i+\mathbf{G}|$, then $\mathbf{k}_i$ lies on the Bragg plane determined by $\mathbf{G}$. In this case we have two degenerate levels, $D_{0i}=1/i0^+$, and the probability diverges. Similar analysis holds when $|\mathbf{k}_f|=|\mathbf{k}_f-\mathbf{G}|$. The degeneracy found at the Bragg plane is lifted, however, by the lattice weak periodic potential, as it is shown in the basic literature (see, for example, the work by Ashcroft and Mermin [12]). Therefore we replace D_{0i} and D_{0f} by

$$D_i=\omega_{\mathbf{k}_i}-\omega_{\mathbf{k}_i+\mathbf{G}}+i|V_{\mathbf{G}}|,$$

$$D_f=\omega_{\mathbf{k}_f}-\omega_{\mathbf{k}_f-\mathbf{G}}+i|V_{\mathbf{G}}|, \tag{21}$$

Rösler *et al.* formula for the form factor follows from a two-band model calculation [4]. Their expression is nonetheless equivalent to our Eq. (19) so far as we consider $0^+\sim|V_{\mathbf{G}}|$, $|V_{\mathbf{G}}|\ll 1$ and we work with D instead of D_0. There are some differences with respect to **G**'s sign, but they are due to working in a reduced or extended zone scheme, and do not produce different results.

III. RESULTS

Results for protons colliding with polycrystalline aluminum are reported here for different possible processes. From now on, we will identify each process considered with an abbreviation. ''ISh'' will stand for electronic excitations from the inner shells of aluminum, ''Bin'' for electronic excitation from the free-electron gas [Eq. (14)], and ''Dec'' for electronic excitation of a nearly free electron due to plasmon decay [Eq. (20)]. Finally, ''Pls'' will stand for plasmon excitation.

$$\mathrm{H}^+ + \mathrm{Al}(nl)\rightarrow \mathrm{H}^+ + \mathrm{Al}^+ + e_{\mathbf{k}_f}, \quad \mathrm{ISh}$$

$$\mathrm{H}^+ + e_{\mathbf{k}_i}(\mathrm{FEG})\rightarrow \mathrm{H}^+ + e_{\mathbf{k}_f}, \quad \mathrm{Bin}$$

$$\mathrm{H}^+ + \mathrm{FEG}\rightarrow \mathrm{H}^+ + \mathrm{FEG}^*, \quad \mathrm{Pls}$$

$$\mathrm{H}^+ + \mathrm{FEG}\rightarrow \mathrm{H}^+ + \mathrm{FEG}^*\rightarrow \mathrm{FEG}^+ + e_{\mathbf{k}_f}, \quad \mathrm{Dec}. \tag{22}$$

The Mermin-Lindhard dielectric response function $\varepsilon_M(q,\omega,\gamma)$ [18] was used to represent the FEG in Eq. (12). The following parameters were considered: the Fermi veloc-

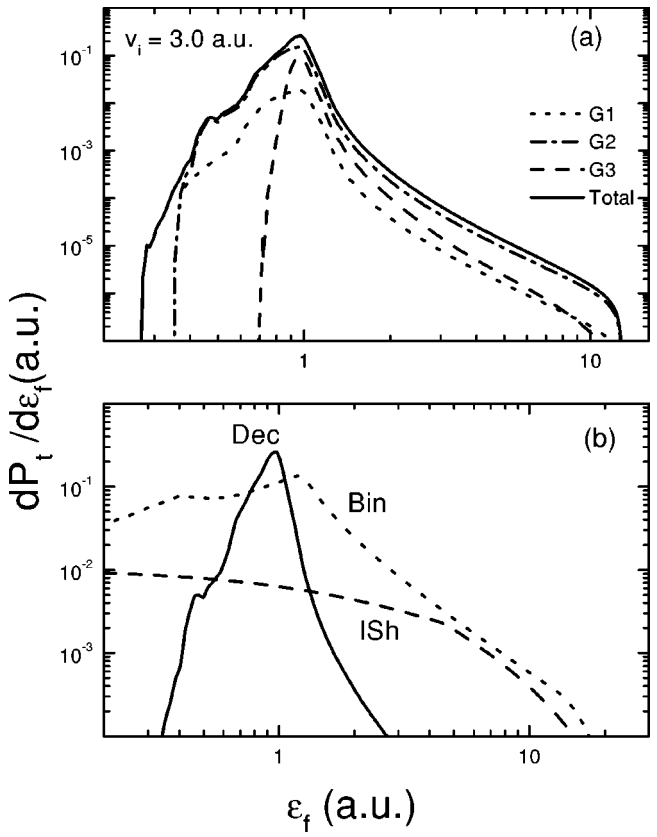

FIG. 4. Single-differential probability as a function of the excited electron final energy for $V_i = 3.0$ a.u. (measured from the bottom of the band). Contributions from different **G** values are discriminated. The notation is similar to Fig. 2.

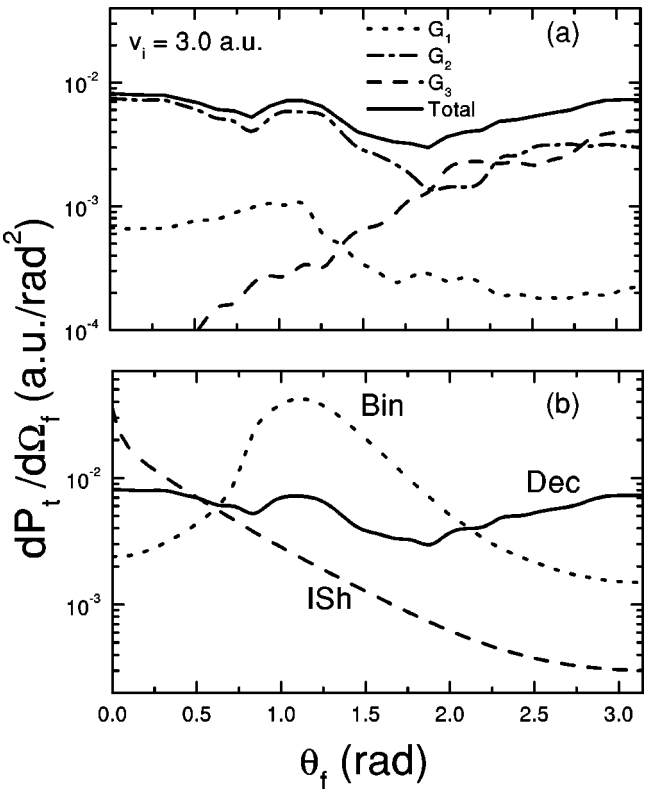

FIG. 5. Single-differential probability as a function of θ_f (excited electron outgoing direction with respect to the projectile intial velocity). Contributions from different **G** values are discriminated. The notation is similar to Fig. 2.

ity $k_F = 0.91$ (plasmon energy $\omega_P = 0.566$), the inverse of the lifetime $\gamma_0 = 0.0375$ (following Arista [19]), and the following lattice parameters:

$$|\mathbf{G}_1| = 1.425(\text{eight neighbors}), \quad |V_{\mathbf{G}_1}| = 0.0089,$$

$$|\mathbf{G}_2| = 1.645(\text{six neighbors}), \quad |V_{\mathbf{G}_2}| = 0.0281,$$

$$|\mathbf{G}_3| = 2.327(\text{twelve neighbors}), \quad |V_{\mathbf{G}_3}| = 0.0271 \quad (23)$$

The first two terms were the ones used by Rösler, and $|V_{\mathbf{G}_3}|$ was determined fitting Shaw results (Table IV of Ref. [11]) with a polynomial to reproduce $|V_{\mathbf{G}_1}|$ and $|V_{\mathbf{G}_2}|$). As we shall show, the influence of the third term $|V_{\mathbf{G}_3}|$ is important, mainly in the high-energy tail. The values for $|V_{\mathbf{G}}|$ depend on the normalization volume considered. We worked with the unit-cell volume.

The polycrystalline structure has been achieved by randomizing the two Euler angles that describe the relative orientation between the projectile velocity and the lattice. The Monte Carlo numerical technique has been used to integrate the differential probabilities. The roughness of the curves shown in this paper is due to the usual standard deviation in the Monte Carlo calculation.

The results for the inelastic collisions of the projectile with the valence electrons, accounting for binary (dP_t^{Bin}) and plasmon (dP_t^{Pls}) excitation per unit time, are presented here, both calculated with the Mermin-Lindhard response function. The total nl inner-shell ionization probability per unit time is included in the figures, $dP_t^{ISh} = dP_t^{2S} + dP_t^{2P}$, P_t^{1S} is negligible in the energy region considered here. They were calculated using the continuum-distorted-wave–eikonal-initial state (CDW-EIS) which makes use of distorted waves in the initial as well as the final channels [20].

A. Total probability and stopping power

In Fig. 2, we show dP_t^{Dec} (i.e., the transition probability per unit time for plasmon decay via electron excitation as calculated in the preceding section) as a function of the projectile velocity v_i. The result we obtain is qualitatively consistent with the data we have used. For the Mermin-Lindhard dielectric response function used here, the inverse of the lifetime $\gamma(q)$ ranges from $\gamma_0 = \gamma(q=0) = 0.0375$ to $\gamma(q_c = 0.67) \sim 2\gamma_0 = 0.075$. Based on the plot for $\varepsilon(q,\omega)$, we know the ion velocity has a minimum value v_{th}, called the threshold velocity under which the projectile cannot generate plasmons directly. For protons on aluminum, $v_{th} = 1.24$. At v_{th}, the projectile generates a plasmon with energy $\omega = \omega_c \sim 0.83$ a.u. and lifetime $\gamma(q_c) = 0.075$, which is near the maximum value obtained for dP_t^{Dec}. As v_i increases, other plasmons with $\omega < \omega_c$ having longer lifetimes (smaller value

of γ) are excited too, and contribute to the total probability; therefore increasing dP_t^{Dec}. Around $v_i \sim 3.0$ a.u., dP_t^{Dec} saturates as plasmons with every allowed energy are excited.

Together with dP_t^{Dec}, we also plot dP_t^{Pls}, dP^{Bin}, and dP^{ISh} [20] to establish a comparison. It is important to note that $dP_t^{Pls} > dP_t^{Dec}$, i.e., the plasmon formation probability is nearly twice as large as the plasmon decay one. This means that it is easier to excite a plasmon than to make it decay via this mechanism. That is, the plasmon excitation rate is higher than the plasmon decay one.

Possibly, values of $|V_{\mathbf{G}_j}|$ could be improved. Also, inclusion of higher terms such as $|V_{\mathbf{G}_4}|$ would increase dP_t^{Dec}, but not significantly, given the decreasing amplitude of the oscillations of the model potential [11]. The value of $|V_{\mathbf{G}_4}|$ is similar to that of $|V_{\mathbf{G}_1}|$, and it is also near a node of the model potential considered. We ran the program including $|V_{\mathbf{G}_4}| = 0.01$ a.u., but found no important corrections to our results.

Another source of uncertainty is the value of γ_0. In Rösler calculations, γ is more sensitive to changes in q. It is calculated with $\gamma_{Ross} = 0.018[1 + 6(q/k_F)^2]$ and $\gamma(q_c) \sim 4\gamma_0$.

We have explored the stability of our results considering the value 0.018 used by Rösler and Brauer [4] (instead of 0.0375), and an increment of 15% was observed.

In Fig. 3 we plot the energy lost per unit time by the projectile (stopping) via binary collisions with the FEG S_t^{Bin}, inner-shell ionization S_t^{ISh} [21], the plasmon formation S_t^{Pls} (which is similar at high velocities to S_t^{Bin} due to the equipartition rule), and the integrated energy of the excited electron via the plasmon decay S_t^{Dec},

$$S_t^{Dec} = \int d\omega\, \omega \int d\mathbf{k}_f \delta(\mathbf{q}\cdot\mathbf{v} - \omega) \frac{dP_t^{Dec}}{d\mathbf{k}_f} \Theta(k_f - k_F). \tag{24}$$

Again it may be seen that nearly one-third of the energy ceded by the projectile to the plasmon per unit time is converted to kinetic energy of the emitted electron.

B. Single-differential spectra in angle and energy

From now on, we will concentrate on protons impinging with $v_i = 3$ (225 keV), where the probability for plasmon decay reaches its maximum. We expect the decay spectrum not to vary much for higher velocities.

Single-differential probabilities as a function of the excited electron energy $dP_t/d\varepsilon_f$, with $\varepsilon_f = k_f^2/2$, are shown in Fig. 4(b) for the three cases considered ending with one electron in the continuum, i.e., plasmon decay, binary, and inner-shell ionization processes. In Fig. 4(a), we discriminate the three different contributions for the plasmon decay due to first, second, and third neighbors in the reciprocal lattice (i.e., **G**'s three lowest values). The $\mathbf{G}_1$ contribution (lowest lattice momentum) is important only for very low energies. $\mathbf{G}_2$ determines the shape of the curve for intermediate ener-

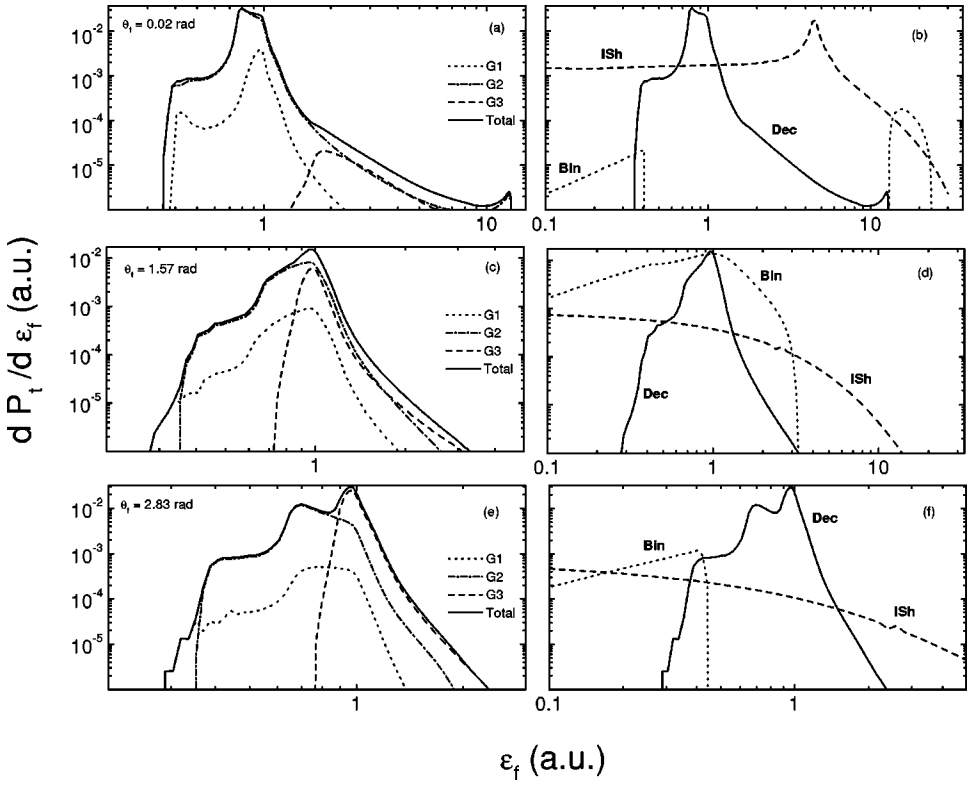

FIG. 6. Double-differential probability as a function of the excited electron final energy (again, measured from the bottom of the band). Three different outgoing directions ($\theta_f = 0.02$, $\theta_f = 1.57$, and $\theta_f = 2.83$ rad) are considered. Contributions from different **G** values are discriminated. The notation is similar to Fig. 2.

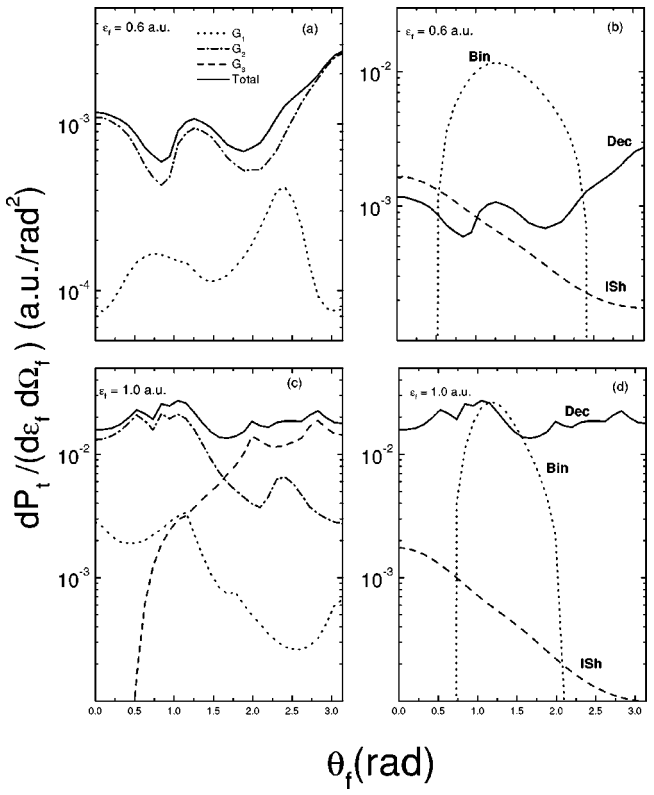

FIG. 7. Double-differential probability as a function of the excited electron outgoing direction. Two-electron final energies are considered: $E_f=0.6$ and $E_f=1.0$ (from the bottom of the band). Contributions from different **G** values are discriminated. The notation is similar to Fig. 2.

gies and, together with $\mathbf{G}_3$, clearly dominates in the high-energy region. The plasmon decay probability clearly presents a peak concentrated around $\varepsilon_f \sim 0.97$ a.u.; dP_t^{ISh} is small in that region and the spectrum is dominated mainly by the valence electrons. We understand this value considering that the excited electron initial energy ε_i is in the interval $0<\varepsilon_i<\varepsilon_F \sim 0.41$ a.u., and the plasmon energy ω is 0.565 a.u.$<\omega<0.83$ a.u. As the excited electron final energy ε_f is given by $\varepsilon_f=\varepsilon_i+\omega$, we find that

$$0.565 \text{ a.u.} < \varepsilon_f < 1.24 \text{ a.u.} \tag{25}$$

In Fig. 4(b), we see that it is in this energy region that most of the electrons are excited. The fact that the peak is actually closer to the upper limit means that excited electrons come from near the Fermi level. Most of the excited plasmons are low-energy ones, and although they have longer lifetimes, it is their decay that determines the peak's position $(0.41+0.565=0.97$ a.u.). The shape of our curves is similar to that obtained by Rösler and Brauer, and the results are of the same order [4].

The most relevant information is found in the angular distribution $dP_t/d\Omega_f$ as observed in Fig. 5(b). While dP_t^{ISh} contributes mainly in the forward direction and dP_t^{Bin} concentrates in a direction perpendicular to the beam, dP_t^{Dec} keeps a nearly spherical symmetry and becomes dominant at backward angles, where $\mathbf{G}_2$ and $\mathbf{G}_3$ contributions are of the same order [see Fig. 5(a)].

C. Double differential spectra

Figure 6 shows the electronic distribution in angle and energy as a function of the electron kinetic energy for three ejection angles as indicated. The **G**-discriminated plots [Figs. 6(a), 6(c), and 6(e)] show that $\mathbf{G}_2$ and $\mathbf{G}_3$ make the main contribution except at the very low-energy tail. At the backward direction [Fig. 6(e)], we find that the $\mathbf{G}_3$ contribution becomes dominant for high energies while $\mathbf{G}_2$ rules in the middle region and $\mathbf{G}_1$ for very low electron energies. Note that three different plasmon peaks can be clearly recognized here, the first two being $\mathbf{G}_2$ peaks and the third a $\mathbf{G}_3$ one. In Figs. 6(b), 6(d), and 6(f), the total plasmon decay contribution is plotted together with binary and inner-shell ones. We see that in the forward and normal directions, inner-shell and binary processes are dominant, leaving plasmon decay as the leading mechanism for electron excitation in the backwards direction. It is important, however, to point out that the transport of the electrons from the point where they are created to the surface and the transmission of the electrons through the surface potential barrier modify both the angle and energy distributions. So, the excitation energy and angle distributions considered here are not the same as the emitted ones (that can be compared with actual experimental data). Note that the $\mathbf{G}_1$ contribution could not be detected since the other two processes are dominant in the low-energy region as observed in Fig. 6(f). $\mathbf{G}_2$ and $\mathbf{G}_3$ contributions can be clearly separated. This could be an interesting region to study the lattice influence.

Figure 7 shows the electronic distribution in angle and energy as a function of the ejection angle for two-electron kinetic energy as indicated, which corresponds to $\varepsilon_f \sim 0.6$ a.u.$\gtrsim \varepsilon_{\min}$ [given by Eq. (25)] and $\varepsilon_f \sim 1.0$ a.u. (around the plasmon decay peak position). Again, the structures follow the trend observed in the previous results. dP_t^{ISh} is enhanced in the forward direction, dP_t^{Bin} is very concentrated and largely dominates the spectrum in the direction perpendicular to the beam, and dP_t^{Dec} shows a nearly symmetric distribution, then leaving the backward direction with plasmon decay as the leading mechanism. For both energies, plasmon decay constitutes the most important mechanism in this direction. It is worth noting that for $\varepsilon_f=0.6$ a.u., the plasmon contribution is determined mainly by $\mathbf{G}_2$; while for $\varepsilon_f=1.0$ a.u., $\mathbf{G}_3$ dominates the backward direction.

IV. CONCLUSIONS

A simple model was developed to describe electron excitation caused by plasmon decay. The T matrix was built using a Born expansion to include the electron-electron interaction to all orders leading to the FEG dielectric response function. All valence electrons were considered free except for the excited ones. This approximation is valid to first order in the projectile charge. The lattice was considered in the momentum-conservation equation, to which it contributes with a reciprocal lattice vector **G**. The weak periodic poten-

tial generated by the lattice was considered as a perturbation on the Bloch electrons. The electronic wave function was approximated using a first-order Born expansion. Our final expression is similar to the one used by Rösler and coworkers, except in minor points.

Our results for the total probability of electron excitation via plasmon decay per unit time account for just one-half of the plasmons excited by the projectile. Further, the kinetic energy of the excited electron is smaller than the energy deposited by the projectile to excite the plasmons. This is due to the fact that the plasmon excitation rate is higher than the plasmon decay one. In the angular and energy spectra, we discriminate the effect of the different **G** values and determine the most favorable conditions for electron excitation due to plasmon decay; that is, low-energy electrons ($\varepsilon_f \sim 1.0$) excited in the backward direction. Plasmon decay dominates here over both inner-shell and binary-ionization processes. The lattice plays a strong role in the excitation of these electrons as it contributes with $\mathbf{G}_3$ (third neighbors in the reciprocal lattice).

ACKNOWLEDGMENTS

We thank Dr. M. S. Gravielle for providing us with the results corresponding to inner shell contributions. This work was done with the financial support of the Universidad de Buenos Aires (Grant No. UBACyT X044) and the Agencia Nacional para la Promoción de la Ciencia y la Tecnología (Grant Nos. PICT98 0303579 and PICT99 0306249). We also thank Dr. M. Rösler for his careful reading of this manuscript and his useful comments about it.

[1] J.L. Gervasoni, Ph.D. thesis, Universidad Nacional de Cuyo, 1992 (unpublished).
[2] M.S. Chung and T.E. Everhart, Phys. Rev. B **15**, 4699 (1977).
[3] M. Rösler and W. Brauer, Phys. Status Solidi B **104**, 161 (1981).
[4] M. Rösler and W. Brauer, Springer Tracts Mod. Phys. **122**, 1 (1991).
[5] M. Rösler, Nucl. Instrum. Methods Phys. Res. B **90**, 537 (1994).
[6] M. Rösler, Appl. Phys. A: Mater. Sci. Process. **A61**, 595 (1995).
[7] V. Heine and I. Abarenkov, Philos. Mag. **9**, 451 (1964).
[8] A.O.E. Animalu, Philos. Mag. **11**, 379 (1965).
[9] A.O.E. Animalu and V. Heine, Philos. Mag. **12**, 1249 (1965).
[10] I.V. Abarenkov and V. Heine, Philos. Mag. **12**, 529 (1965).
[11] R.W. Shaw, Jr., Phys. Rev. **174**, 769 (1968).
[12] N.W. Ashcroft and N.D. Mermin, *Solid State Physics* (Holt, New York, 1976).
[13] M. Rösler and W. Brauer, Phys. Status Solidi B **104**, 575 (1981).
[14] J. Lindhard, K. Dan. Vidensk. Selsk. Mat. Fys. Medd. **28**, 8 (1954).
[15] R.H. Ritchie, Phys. Rev. **114**, 644 (1959).
[16] D. Arbó and J. Miraglia, Phys. Rev. A **58**, 2970 (1998).
[17] H.A. Bethe and E.E. Salpeter, *Quantum Mechanics of One and Two Electron Atoms* (Springer-Verlag, Berlin, 1957).
[18] D. Mermin, Phys. Rev. B **1**, 2362 (1970).
[19] N.R. Arista, Phys. Rev. A **49**, 1885 (1994).
[20] M.S. Gravielle (private communication).
[21] D.G. Arbó, M.S. Gravielle, and J.E. Miraglia, Phys. Rev. A **62**, 032901 (2000).